STATISTICS, OPTIMIZATION AND INFORMATION COMPUTING
Stat., Optim. Inf. Comput., Vol. **14**, month 2025, pp 0–14.
Published online in International Academic Press (www.IAPress.org)

Electrical Parameter Estimation in Solar Cells Using Single-, Double-, and Three-Diode Models

Jenny Catalina Garzón-Acosta, Oscar Danilo Montoya*, César Leonardo Trujillo-Rodríguez

Facultad de Ingeniería, Universidad Distrital Francisco José de Caldas, Bogotá D.C. 110121, Colombia

Abstract Accurately modeling photovoltaic (PV) systems is essential for performance optimization and reliability assessment in renewable energy applications. This study proposes a novel hybrid methodology for parameter estimation in single-, double-, and three-diode PV models, which combines the equilibrium optimization algorithm (EOA) with the Newton-Raphson method to solve the implicit model equations. This approach was implemented in Python and validated using experimental current-voltage (I-V) data from the Kyocera KC200GT solar module. The objective function aimed to minimize the root mean square error (RMSE) between simulated and measured curves, wherein current values were numerically computed via the Newton-Raphson method for each candidate solution. To evaluate the performance of the models, comparisons were carried out under standard testing conditions (STC) with an irradiance level of 1000 W/m^2. The double-diode model reported the lowest RMSE value under these conditions (RMSE=0.0416 A), confirming its superior accuracy and adequate balance between complexity and performance. Additionally, two lower irradiance levels (800 W/m^2 and 400 W/m^2) were analyzed in order to assess the consistency of the estimated parameters, *i.e.*, the series resistance R_s, shunt resistance R_sh, and ideality factors (n_1, n_2, n_3). This extended analysis revealed that the R_sh parameter exhibits high variability in the three models, with STC showing the greatest deviation (63.28). This further supports the robustness of the proposed method, particularly in the case of the double-diode model. Overall, the hybrid EOA–Newton–Raphson strategy provides a reliable and flexible framework for nonlinear parameter identification in PV systems.

Keywords Metaheuristic optimization, Parameter estimation, Photovoltaic modeling, Python programming

AMS 2010 subject classifications 62J07

DOI:10.19139/soic-2310-5070-2856

Nomenclature

Functions

$\varepsilon(\phi)$	Objective function (sum of the squared errors between I_{sim} and I_{exp})
RMSE	Root mean square error between simulated and experimental current values [A]

Models

DD	Double-diode PV model
EOA	Equilibrium optimizer algorithm
NRM	Newton–Raphson method
SD	Single-diode PV model

*Correspondence to: O. D. Montoya (Email: odmontoyag@udistrital.edu.co). Facultad de Ingeniería, Universidad Distrital Francisco José de Caldas, Bogotá D.C. 110121, Colombia.

ISSN 2310-5070 (online) ISSN 2311-004X (print)

TD Three-diode PV model

Parameters

ϕ Vector of parameters to be optimized

C Initial population in heuristic approaches

F Exponential term to update the rule in the EOA

G Irradiance or solar insolation [W/m^2]

I_{01} Reverse saturation current for diffusion losses in the neutral region [A]

I_{02} Reverse saturation current for recombination in the depletion region [A]

I_{03} Reverse saturation current for surface or edge recombination [A]

I_{ph} Photogenerated current by photoelectric effect [A]

n_1 Ideality factor for the diffusion region

n_2 Ideality factor for the depletion region

n_3 Ideality factor for surface recombination

N_s Number of series-connected cells

R_s Series resistance [Ω]

R_{sh} Shunt resistance [Ω]

T Cell temperature [K]

V_t Thermal voltage, $V_t = \frac{kT}{q}$ [V]

Variables

I Terminal current of the photovoltaic cell [A]

$I_{\text{exp},k}$ Experimentally measured current at the k-th data point [A]

$I_{\text{sim}}(V_k, \phi)$ Simulated current from the PV model for voltage V_k and the parameters ϕ [A]

V Terminal voltage of the photovoltaic cell [V]

V_k Voltage applied at the k-th experimental data point [V]

1. Introduction

The current ecological landscape reflects the consequences of a consumption model that heavily relies on the exploitation of finite natural resources. In this context, the intensive use of fossil fuels poses a dual challenge: their significant environmental impact and their limited long-term availability [1]. In response, the global energy transition has increasingly favored renewable energy sources, with photovoltaic (PV) systems leading the expansion of the installed capacity for electricity generation [2]. Solar energy is particularly relevant due to its global availability, sustainability, and potential to decarbonize the energy sector.

Accurately modeling the behavior of PV systems is essential for analyzing and optimizing their performance. Various electrical models—namely the single-diode, double-diode, and three-diode configurations—have been developed to represent solar cell behavior with increasing levels of detail. The single-diode model (SDM) is widely employed in PV research due to its simplicity and its ability to adequately capture the nonlinear current-voltage (I–V) characteristics of solar cells at a relatively low computational cost [3]. In contrast, the double-diode model (DDM) introduces a second diode to account for two distinct recombination mechanisms: diffusion and depletion-region recombination. While this enhances physical accuracy, it also increases model complexity, as it requires estimating seven parameters that are sensitive to environmental conditions [4]. The three-diode model (TDM)

further improves this representation by incorporating additional loss mechanisms, both optical and electrical. Electrical losses stem from the series resistance (R_s) due to wire and contact conduction, as well as from the shunt resistance (R_{sh}), representing leakage currents. Optical losses, on the other hand, are associated with carrier recombination in the depletion region and grain boundaries, which are modeled through three parallel diodes [5].

Several studies have adopted hybrid approaches that combine analytical techniques with optimization algorithms in order to estimate the unknown parameters of PV models. Among the most commonly used metaheuristics are genetic algorithms (GAs), particle swarm optimization (PSO), and gray wolf optimization (GWO), which are typically implemented in MATLAB [5]. More recent research has focused on hybrid metaheuristic strategies to improve parameter estimation, particularly for more complex models such as the TDM. A notable example is the TERIME algorithm, which integrates differential evolution, Gaussian-based local refinement, and memory-based adaptation to balance exploration and exploitation. Although this approach incurs a higher computational cost, it provides improved accuracy and robustness [6].

This work proposes a novel hybrid strategy that combines the equilibrium optimization algorithm (EOA) with the Newton-Raphson method (NRM) to solve the implicit model equations. This approach was implemented entirely in Python due to its computational efficiency, open-source ecosystem, and flexibility. To the best of our knowledge, this is the first study to report the integration of the EOA with the NRM for estimating parameters in single-, double-, and three-diode PV models. The EOA was selected for its ability to efficiently explore high-dimensional, nonlinear search spaces. The procedure begins with a random initialization of candidate solutions within physically plausible bounds, as reported in the literature [7], followed by an iterative process aimed at reaching an equilibrium state. The quality of each solution is evaluated using the root mean square error (RMSE) between the simulated and experimental I–V curves, using reference data obtained from the KC200GT module. The output current for each candidate solution is computed using the NRM, ensuring numerical precision and convergence reliability throughout the optimization process.

The remainder of this paper is organized as follows. Section 2 describes the physical principles and component-level interpretations of PV cell models. Section 3 presents the mathematical formulations of the single-, double-, and three-diode configurations, highlighting their increasing levels of model complexity. Section 4 defines the nonlinear optimization problem used for parameter estimation based on experimental I–V data. Section 5 details the proposed hybrid solution methodology that integrates the EOA and the NRM. Section 6 introduces the test system used, *i.e.*, the Kyocera KC200GT module, and outlines the experimental data and parameter bounds used for model calibration. Section 7 provides a comprehensive numerical validation and performance comparison of the three models, and, finally, Section 8 presents the main conclusions of this research and discusses potential directions for future work.

2. Photovoltaic cell models

PV cell models are mathematical representations that characterize the electrical behavior of solar cells under illumination [8]. These models serve as essential tools for predicting the I-V characteristics of PV devices, allowing researchers and engineers to evaluate performance, optimize energy conversion, and diagnose faults under varying environmental conditions. Regardless of model complexity, the fundamental physical mechanisms governing the operation of a solar cell remain consistent. These include photocurrent generation as a result of photon absorption, charge carrier transport through the semiconductor material, and various recombination processes that limit the efficiency of charge collection. Moreover, practical PV modules exhibit parasitic effects such as resistive losses due to internal wiring and contacts (which are modeled via the series resistance), as well as leakage currents across the $p--n$ junction, caused by imperfections or degradation (modeled via shunt resistance) [9].

To ensure a coherent analysis across different model architectures, it is useful to identify and interpret the common electrical components involved in each configuration. Photogenerated current, for instance, represents the primary current source and depends linearly on solar irradiance and nonlinearly on temperature. Diodes model the nonlinear recombination of carriers in distinct regions of the solar cell, ranging from the quasi-neutral zone to the depletion region and the surface or edge interfaces. The series and shunt resistances, although often

treated as secondary effects, play a critical role in shaping the fill factor and determining the maximum power output. By establishing a unified physical framework, as summarized in Table 1, this study enables a comparative assessment of the SDM, DDM, and TDM while maintaining a consistent basis for parameter interpretation. This foundation is crucial for both the optimization procedure and the subsequent performance evaluation of the proposed methodology.

Table 1. Physical interpretation of the components in PV cell models

Component	Physical interpretation
Photogenerated current (I_{ph})	It represents the current generated by the PV effect when photons are absorbed by the semiconductor. It is directly proportional to solar irradiance and influenced by temperature. I_{ph} serves as the primary source of electrical power in the cell [10].
Diode losses (I_{ni}, n_i)	They model recombination mechanisms through exponential terms. The SDM uses one saturation current (I_{ni}) and one ideality factor (n), while the SDM and the TDM assign a specific pair (I_{ni}, n_i) to each recombination path: • I_{01}: diffusion in quasi-neutral regions • I_{02}: recombination in the depletion region • I_{03}: surface or edge recombination The ideality factor indicates the dominant transport mechanism (diffusion, recombination, tunneling) depending on the current level [11].
Series resistance (R_s)	It models resistive losses due to bulk semiconductor resistance, contact resistance, and metallic interconnections. High R_s values lead to a reduced fill factor and a lower output power [12].
Shunt resistance (R_{sh})	It accounts for leakage currents due to defects, cracks, or impurities. A low R_{sh} degrades performance by reducing the open-circuit voltage and efficiency [12].

3. Mathematical modeling

Accurately modeling PV cells is essential for predicting their performance and optimizing energy conversion systems. Several electrical models have been proposed in the literature, each offering varying degrees of complexity and physical detail. This section presents the mathematical formulations of three widely studied configurations: the SDM, the DDM, and the TDM. These models differ primarily in their number of recombination mechanisms, but they share a common structure based on a photogenerated current source, one or more diodes, and resistive losses. Their corresponding I-V equations are inherently nonlinear and transcendental, requiring numerical solution methods for practical implementation.

3.1. Single-diode model

The SDM is a simplified yet widely adopted representation of the electrical behavior of PV cells. It comprises a photogenerated current source (I_{ph}), an ideal diode to account for recombination effects, and two resistive elements: a series resistance (R_s) representing internal conduction losses and a shunt resistance (R_{sh}) modeling leakage pathways across the $p--n$ junction [13]. This configuration enables the accurate modeling of the I–V characteristics of a solar cell under varying environmental conditions.

The output current of the cell is governed by a nonlinear transcendental equation that incorporates diode behavior, resistive effects, and temperature-dependent parameters. The SDM equation is presented below.

$$I = I_{\text{ph}} - I_{01}\left(e^{\frac{V+IR_s}{n_1 V_t}} - 1\right) - \frac{V + IR_s}{R_{\text{sh}}} \tag{1}$$

Here, I and V denote the terminal current and voltage, respectively; I_{01} is the reverse saturation current of the diode; n_1 is the ideality factor that reflects the recombination mechanisms; and V_t is the thermal voltage [14]. The nonlinear dependence of current on both voltage and itself (via IR_s) makes analytical solutions impractical, necessitating numerical methods (such as the NRM) for accurately computing the I–V curve [15]. The configuration of the aforementioned parameters is shown in Figure 1.

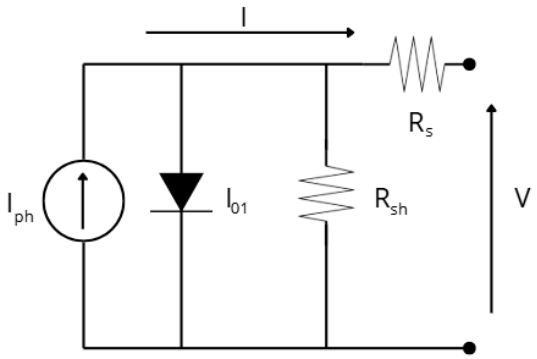

Figure 1. Equivalent circuit of the SDM for a PV cell

3.2. Double-diode model

The DDM offers an enhanced representation of PV cell behavior when compared to the SDM, as it accounts for two distinct recombination mechanisms. Specifically, it introduces a diffusion diode to model carrier losses in the quasi-neutral regions of the semiconductor, as well as a second diode to capture recombination phenomena within the depletion region [8, 16]. The equivalent circuit consists of both diodes connected in parallel with the photogenerated current source. This configuration is further augmented by a series resistance (R_s), which accounts for ohmic losses in the bulk material and contacts, and a shunt resistance (R_{sh}) representing leakage currents due to manufacturing imperfections. The output current, based on the parameters described above, is expressed by Equation (2).

$$I = I_{\text{ph}} - I_{01}\left(e^{\frac{V+IR_s}{n_1 V_t}} - 1\right) - I_{02}\left(e^{\frac{V+IR_s}{n_2 V_t}} - 1\right) - \frac{V + IR_s}{R_{\text{sh}}} \tag{2}$$

Here, I and V denote the output current and voltage of the PV cell, respectively; I_{ph} is the photogenerated current; I_{01} and I_{02} represent the saturation currents associated with the diffusion and recombination diodes; n_1 and n_2 are their corresponding ideality factors; and V_t is the thermal voltage.

The recombination current $-I_{02}\left(e^{\frac{V+IR_s}{n_2 V_t}} - 1\right)$ models the carrier losses in the depletion region of the $p--n$ junction [17]. Although the magnitude of I_{02} is typically smaller than that of I_{01}, its influence becomes particularly significant under low-irradiance conditions or in the presence of structural defects within the cell [18]. The complete configuration of these parameters is illustrated in Figure 2.

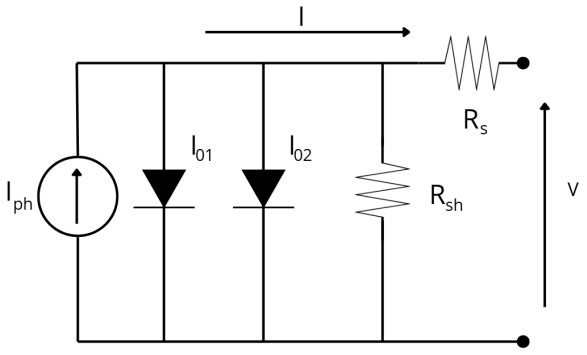

Figure 2. Equivalent circuit of the DDM for a PV cell

3.3. Three-diode model

The TDM extends the physical accuracy of PV cell modeling by incorporating an additional recombination mechanism, thereby offering a more refined representation than the SDM and the DDM. This configuration includes three diodes in parallel with a photogenerated current source, along with a series resistance (R_s) and a shunt resistance (R_{sh}) to represent ohmic and leakage losses, respectively. Each diode in the model accounts for a distinct recombination path: diffusion in the quasi-neutral region, recombination in the depletion region, and surface or edge recombination due to grain boundaries or passivation defects [19].

The mathematical formulation of the TDM is given by (3):

$$I = I_{\text{ph}} - I_{01}\left(e^{\frac{V+IR_s}{n_1 V_t}} - 1\right) - I_{02}\left(e^{\frac{V+IR_s}{n_2 V_t}} - 1\right) - I_{03}\left(e^{\frac{V+IR_s}{n_3 V_t}} - 1\right) - \frac{V + IR_s}{R_{\text{sh}}} \tag{3}$$

Here, I_{01}, I_{02}, and I_{03} denote the saturation currents associated with diffusion, depletion-region recombination, and surface or edge recombination, respectively. Their corresponding ideality factors are denoted by n_1, n_2, and n_3. The third diode term, $-I_{03}\left(e^{\frac{V+IR_s}{n_3 V_t}} - 1\right)$, accounts for recombination losses occurring at the interfaces and grain boundaries, which may result from imperfect surface passivation or material discontinuities. Although this term typically represents a relatively small current, its inclusion enhances the model's accuracy in replicating experimental I–V behavior across a wider range of operating conditions [19]. The electrical configuration of the diodes and the associated resistances is illustrated in Figure 3.

As in the SDM and the DDM, the nonlinear and implicit nature of this equation necessitates numerical solution techniques (such as the NRM) for evaluating the output current across the operating voltage range.

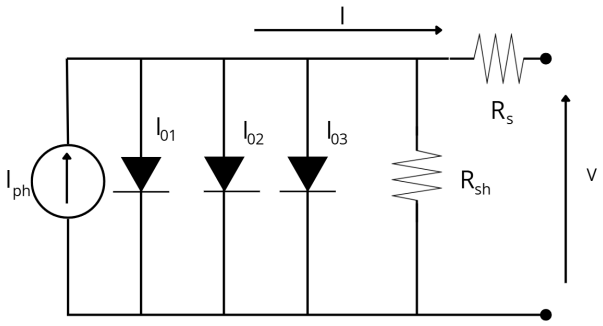

Figure 3. Equivalent circuit of the TDM for a PV cell

4. Optimization problem formulation

The identification of electrical parameters in the SDM, DDM, and TDM is formulated as a nonlinear optimization problem. The goal is to determine the parameter vector ϕ that best reproduces the experimental behavior of the PV module by minimizing the discrepancy between the model-predicted and measured I–V characteristics [20].

To this effect, the objective function defined in Equation (4) is used, which is based on the sum of squared errors (SSE) between the simulated current values and the corresponding experimental measurements taken at each voltage point.

$$\varepsilon(\phi) = \sum_{k=1}^{N} \left(I_{\text{sim}}(V_k, \phi) - I_{\text{exp},k}\right)^2 \tag{4}$$

Here, ϕ denotes the parameter vector to be optimized; V_k is the voltage applied at the k-th experimental data point; $I_{\text{exp},k}$ represents the current measured at said point; and $I_{\text{sim}}(V_k, \phi)$ is the corresponding simulated current, computed by the PV model using the parameters ϕ. The index k runs from 1 to N, where N is the total number of

experimental samples for this case. Thus, the objective function $\varepsilon(\phi)$ quantifies the cumulative deviation between the model and the experimental I–V data. Minimizing it leads to the optimal set of parameters that best fit the observed behavior of the PV module.

The number and nature of the parameters depend on the chosen model:

- SDM: $\phi = \{I_{ph}, I_{01}, R_s, R_{sh}, n_1\}$
- DDM: $\phi = \{I_{ph}, I_{01}, I_{02}, R_s, R_{sh}, n_1, n_2\}$
- TDM: $\phi = \{I_{ph}, I_{01}, I_{02}, I_{03}, R_s, R_{sh}, n_1, n_2, n_3\}$

The current I_{sim} cannot be obtained in closed form due to the implicit and nonlinear structure of the governing I–V equations. Therefore, for each candidate parameter set generated during optimization, the current must be numerically computed using an iterative technique [15]. In this work, the NRM is used for that purpose.

Note that the optimization problem is solved using the EOA [21], which efficiently explores the parameter space to find the configuration that minimizes the total error between the simulated and experimental curves.

5. Solution methodology

This work applies a metaheuristic strategy to estimate the electrical parameters of the single-, double-, and three-diode PV models. This methodology integrates a numerical technique and an optimization algorithm to fit the simulated I-V curve to experimental data by minimizing a defined objective function [22]. Here, the EOA is used for parameter estimation in the SDM, DDM, and TDM, in combination with the NRM for numerically solving the current at each point of the I-V curve. Integrating this approach allows for a robust and efficient search for the global optimum within the parameter space, overcoming the challenges posed by local minima which are often encountered while using traditional optimization techniques. Coupling our strategy with the NRM ensures a precise computation of the current values corresponding to each voltage level, thereby improving the accuracy of the overall model fitting process [23]. This combined approach facilitates the extraction of more reliable and physically consistent parameter sets, which are crucial for the accurate simulation, analysis, and optimization of PV system performance under varying environmental conditions. Furthermore, the flexibility of this methodology enables its application in different PV modules and experimental setups, making it a comprehensive tool for researchers and engineers working in the field of PV modeling and diagnostics.

The EOA simulates the dynamic equilibrium behavior of particles in a solution. The process begins by generating a random initial population of candidate solutions within the lower and upper bounds defined for each model. This step is mathematically expressed in Equation (5).

$$C_i^{\text{initial}} = C_{\min} + \text{rand}_i \cdot (C_{\max} - C_{\min}) \tag{5}$$

In this implementation, a simplified version of the EOA was adopted. Instead of using the original time-varying exponential concentration factor, the update factor F was defined as shown in Equation (6).

$$F = e^{-\frac{m}{m_{\max}}} \cdot \text{rand} \tag{6}$$

where m is the current iteration, $m_{\max}$ is the maximum number of iterations, and `rand` is a random vector with uniformly distributed values in the $[0, 1]$ interval. This simplified approach reduces the complexity of the original model while maintaining the essence of the candidate solutions' dynamic behavior during the optimization process.

The position update formula for each agent is given by (7).

$$C_i^{\text{new}} = C_i + F \cdot (C_{eq} - C_i) \tag{7}$$

The fitness of each candidate is evaluated using the SSE between the simulated and experimental current values, as shown in Equation (8).

$$\varepsilon = \sum_{k=1}^{N} \left(I_k^{\text{sim}} - I_k^{\text{exp}}\right)^2 \tag{8}$$

To compute I_k^{sim}, the current equation is numerically solved using the NRM. For the TDM, the current is defined by a nonlinear equation, as shown in (9).

$$I = I_{ph} - \sum_{i=1}^{3} I_{ni}\left(e^{\frac{V+IR_s}{n_i V_t}} - 1\right) - \frac{V + IR_s}{R_{sh}} \tag{9}$$

Since this equation is implicit in I, the NRM is used iteratively, as shown in Equation (10).

$$I_{k+1} = I_k - \frac{f(I_k)}{f'(I_k)}, \tag{10}$$

where $f(I_k)$ represents the nonlinear current equation, and $f'(I_k)$ is its derivative with respect to current. This procedure is applied at each voltage point in the experimental I-V data.

Finally, model accuracy is evaluated using the RMSE, as defined in Equation (11).

$$\text{RMSE} = \sqrt{\frac{1}{N}\sum_{k=1}^{N}\left(I_k^{\text{sim}} - I_k^{\text{exp}}\right)^2} \tag{11}$$

The NRM is executed for each voltage point to numerically compute the simulated current values based on the candidate's parameters. Thus, this method acts as an internal evaluator that provides the necessary current values to assess the accuracy of each solution proposed by the EOA. While the EOA guides the search throughout the parameter space, the NRM ensures that the objective function is evaluated with high numerical precision, enabling accurate convergence towards the optimal parameter set.

6. Test system: Kyocera KC200GT

To validate the proposed parameter estimation methodology, the Kyocera KC200GT commercial PV module was selected. This monocrystalline silicon module is commonly used in academic research and industrial benchmarking studies due to its well-documented electrical performance and reliability under standardized test conditions [14]. The KC200GT consists of 54 series-connected cells and delivers a nominal maximum power of 200 W under standard testing conditions (STC), which correspond to an irradiance of 1000 W/m^2 and a cell temperature of 25 °C.

In addition to the standard irradiance level of 1000 W/m^2, simulations were also conducted for 800 W/m^2 and 400 W/m^2, with the aim of evaluating model performance under varying environmental conditions.

The experimental I–V data used for the extraction of model parameters are summarized in Tables 2, 3, and 4, which correspond to irradiance levels of 1000 W/m^2, 800 W/m^2, and 400 W/m^2. These data points serve as the reference for calibrating the single-, double-, and three-diode models through nonlinear optimization. Additionally, Table 6 presents the parameter bounds employed in the optimization process.

To construct the experimental I–V curve used in this study, key electrical parameters were extracted directly from the datasheet of the Kyocera KC200GT module. Specifically, the short-circuit current, the open-circuit voltage, and the current and voltage at the maximum power point were utilized as anchor values. The intermediate data points were interpolated based on the graphical profile presented in the datasheet, ensuring a realistic reconstruction of the module's I–V behavior under STC. The resulting dataset is summarized in Table 2.

For the sake of comparison, Table 5 reports the parameter values obtained using the circle search algorithm (CSA) and the transient search optimizer (TSO), two recent metaheuristic techniques introduced in 2022 and 2020, respectively [5]. These algorithms were selected due to their demonstrated effectiveness in PV parameter estimation tasks and their relevance in recent literature. Their inclusion provides a meaningful benchmark against which the proposed method can be evaluated.

The parameter bounds necessary for executing the EOA are shown in Table 6.

Table 2. Experimental I-V data for the Kyocera KC200GT module at **1000 W/m^2**

Voltage (V)	0.0	4.8	9.6	14.4	19.2	24.0	28.8
Current (A)	8.24	8.21	8.19	8.16	8.11	7.83	5.75
Voltage (V)	0.8	5.6	10.4	15.2	20.0	24.8	29.6
Current (A)	8.23	8.21	8.18	8.16	8.09	7.67	4.80
Voltage (V)	1.6	6.4	11.2	16.0	20.8	25.6	30.4
Current (A)	8.23	8.20	8.18	8.15	8.07	7.51	3.86
Voltage (V)	2.4	7.2	12.0	16.8	21.6	26.4	31.2
Current (A)	8.23	8.20	8.18	8.14	8.03	7.20	2.45
Voltage (V)	3.2	8.0	12.8	17.6	22.4	27.2	32.0
Current (A)	8.22	8.20	8.17	8.14	7.99	6.89	1.04
Voltage (V)	4.0	8.8	13.6	18.4	23.2	28.0	—
Current (A)	8.21	8.20	8.16	8.12	7.91	6.32	—

Table 3. Experimental I–V data for the Kyocera KC200GT module at **800 W/m^2**

Voltage (V)	0.0	4.8	9.6	14.4	19.2	24.0	28.8
Current (A)	6.50	6.50	6.49	6.41	6.38	6.23	5.20
Voltage (V)	0.8	5.6	10.4	15.2	20.0	24.8	29.6
Current (A)	6.50	6.50	6.49	6.40	6.38	6.18	4.70
Voltage (V)	1.6	6.4	11.2	16.0	20.8	25.6	31.4
Current (A)	6.50	6.50	6.47	6.40	6.35	6.03	3.00
Voltage (V)	2.4	7.2	12.0	16.8	21.6	26.4	32.3
Current (A)	6.50	6.50	6.46	6.39	6.32	5.85	1.56
Voltage (V)	3.2	8.0	12.8	17.6	22.4	27.2	33.0
Current (A)	6.50	6.50	6.44	6.39	6.29	5.675	0.00
Voltage (V)	4.0	8.8	13.6	18.4	23.2	28.0	—
Current (A)	6.50	6.50	6.43	6.39	6.26	5.45	—

Table 4. Experimental I-V data for the Kyocera KC200GT module at **400 W/m^2**

Voltage (V)	0.0	4.8	9.6	14.4	19.2	24.0	28.8
Current (A)	3.33	3.33	3.33	3.32	3.29	3.18	2.35
Voltage (V)	0.8	5.6	10.4	15.2	20.0	24.8	29.6
Current (A)	3.33	3.33	3.32	3.32	3.28	3.15	1.90
Voltage (V)	1.6	6.4	11.2	16.0	20.8	25.6	30.4
Current (A)	3.33	3.33	3.32	3.31	3.26	3.05	1.30
Voltage (V)	2.4	7.2	12.0	16.8	21.6	26.4	31.2
Current (A)	3.33	3.33	3.32	3.30	3.23	2.99	0.70
Voltage (V)	3.2	8.0	12.8	17.6	22.4	27.2	32.0
Current (A)	3.33	3.33	3.32	3.30	3.20	2.88	0.00
Voltage (V)	4.0	8.8	13.6	18.4	23.2	28.0	—
Current (A)	3.33	3.33	3.32	3.29	3.20	2.72	—

Table 5. Electrical parameters for the TDM as obtained with the CSA and TSO

Parameter	CSA	TSO
n_1	1.00000	1.42169
n_2	1.45200	1.32019
n_3	2.00000	1.25132
I_{o1} (A)	3.04846×10^{-10}	2.01110×10^{-10}
I_{o2} (A)	1.68208×10^{-7}	8.32234×10^{-11}
I_{o3} (A)	1.00000×10^{-12}	4.81327×10^{-8}
R_s (Ω)	0.291994	0.252107
R_p (Ω)	500.00	285.97
I_{ph} (A)	8.19712	8.25201
RMSE (A)	**0.03238**	**0.04444**

Table 6. Parameter bounds for the Kyocera KC200GT's TDM

Parameter	Lower bound	Upper bound
I_{ph} (A) – 1000 W/m^2	6.0	9.0
I_{ph} (A) – 800 W/m^2	5.0	8.0
I_{ph} (A) – 400 W/m^2	2.0	5.0
I_{01}, I_{02}, I_{03} (A)	1×10^{-9}	1×10^{-6}
R_s (Ω)	0.1	0.5
R_{sh} (Ω)	200	800
n_1, n_2, n_3	1.0	2.0

7. Numerical validation

To assess the performance of each model configuration, a comprehensive numerical validation was conducted using the experimental I-V data from the Kyocera KC200GT PV module. The objective was to quantify and compare the accuracy of the SDM, DDM, and TDM when estimating their parameters through the EOA. All model configurations were evaluated independently under identical initial conditions and optimization settings in order to ensure consistency and fairness in the comparison. The RMSE was employed as the primary performance metric, providing a robust measure of the deviation between the simulated and experimental curves.

The computational implementation was carried out in Python, version 3.12.8 (64-bit). All simulations were executed on a personal computer equipped with an Intel(R) Core(TM) i5-5200U CPU (running at 2.20 GHz), 8 GB of RAM, and Microsoft Windows 10 (64-bit). The EOA was configured with a population size of 30 and a maximum of 500 iterations. Additionally, the NRM was employed to numerically solve the implicit current equations, which lack closed-form solutions. This iterative approach was essential for accurately simulating the I-V curves and assessing the quality of fit during the optimization process. The results, including the estimated parameters, convergence times, and RMSE values for each model configuration, are summarized in Table 7.

Table 7. Estimated parameters, convergence time, and RMSE for each model (EOA-NRM)

Parameter	SDM	DDM	TDM
I_{ph} (A)	8.20359	8.21306	8.21530
I_{01} (A)	6.07689×10^{-7}	8.71437×10^{-7}	6.67523×10^{-7}
I_{02} (A)	–	3.10541×10^{-7}	7.83895×10^{-7}
I_{03} (A)	–	–	5.37417×10^{-7}
R_s (Ω)	0.29139	0.27152	0.29792
R_{sh} (Ω)	515.92	393.04	483.51
n or n_1	1.4377	1.75619	1.61631
n_2	–	1.38294	1.58845
n_3	–	–	1.48960
RMSE (A)	0.0636	0.0416	0.0980

Based on the updated results, the DDM exhibited the lowest RMSE (0.0416 A), demonstrating the highest accuracy in fitting the experimental I-V data. This improved performance stems from the model's ability to better capture recombination mechanisms through the inclusion of a second exponential term, enhancing the model's flexibility without excessive complexity.

The SDM achieved a competitive error of 0.0636 A. Despite its simplicity and reduced parameter count, it effectively reproduced the overall electrical behavior of the solar cell while offering computational efficiency. In all cases, the photogenerated current remained consistently close to 8.2 A, reflecting its robustness across different model structures.

In contrast, the TDM, although more detailed, reported a higher error (0.098 A). Its added complexity, intended to capture additional recombination and interface effects, may have led to overfitting or instability due to parameter coupling and increased dimensionality.

As for the resistive parameters, the highest shunt resistance was observed in the single-diode case (515.9 Ω), followed by the three-diode (483.5 Ω) and double-diode models (393.0 Ω), suggesting differences in the way in which each configuration compensates for leakage currents. The series resistance remained stable across models, ranging from 0.27 to 0.30 Ω.

Overall, while the simplest model offers a favorable trade-off between accuracy and efficiency, the double-diode structure provides an enhanced descriptive capacity when greater detail is required. The TDM, despite its theoretical advantages, failed to provide improved accuracy under the tested conditions, possibly due to the optimizer's behavior in flat regions or to the imposed boundary constraints.

To further evaluate the reliability of the parameter estimation procedure, the standard deviation of the extracted values was analyzed over multiple runs using the method implemented in Python (EOA-NRM), and a comparison against the results obtained from the CSA and TSO was performed. Table 8 presents the standard deviations obtained for each parameter in the SDM, DDM, and TDM. Lower standard deviation values indicate greater consistency and robustness in the optimization outcomes.

Table 8. Standard deviation of the parameters the for SDM, DDM, and TDM

Parameter	**SDM**	**DDM**	**TDM**
I_{ph}	0.0245	0.0231	0.0228
I_{01}	0.1265	4.1068e-7	3.1455e-7
I_{02}	–	1.2689e-7	3.3693e-7
I_{03}	–	–	2.4279e-7
R_s (Ω)	0.0187	0.0163	0.0203
R_{sh} (Ω)	104.85	87.38	97.24
n	0.2026	–	–
n_1	–	0.3094	0.2572
n_2	–	0.0539	0.1096
n_3	–	–	0.3123
RMSE (A)	0.0129	0.0051	0.0286

Among the three models, the configuration with two diodes exhibited the most stable results, particularly regarding the series resistance and the ideality factors associated with each diode. This suggests that the model's moderate complexity contributes to a more reliable convergence of the optimization algorithm. In contrast, the SDM and the TDM showed greater variability in key parameters such as the shunt resistance and the photogenerated current. These differences may be attributed to the structural limitations of the simpler model or to the over-parameterization effects of the more complex one. Overall, the results emphasize the necessary balance between model accuracy and parameter stability in the context of nonlinear identification.

Figure 4 illustrates the simulated I-V characteristics obtained from the SDM, DDM, and TDM, in comparison with the experimental data.

Overall, the three configurations show a strong agreement with the measured behavior of the PV module across most of the voltage range, successfully replicating the general nonlinear profile of the curve. Notably, minor deviations emerge near the region corresponding to the maximum power point, particularly in the descending

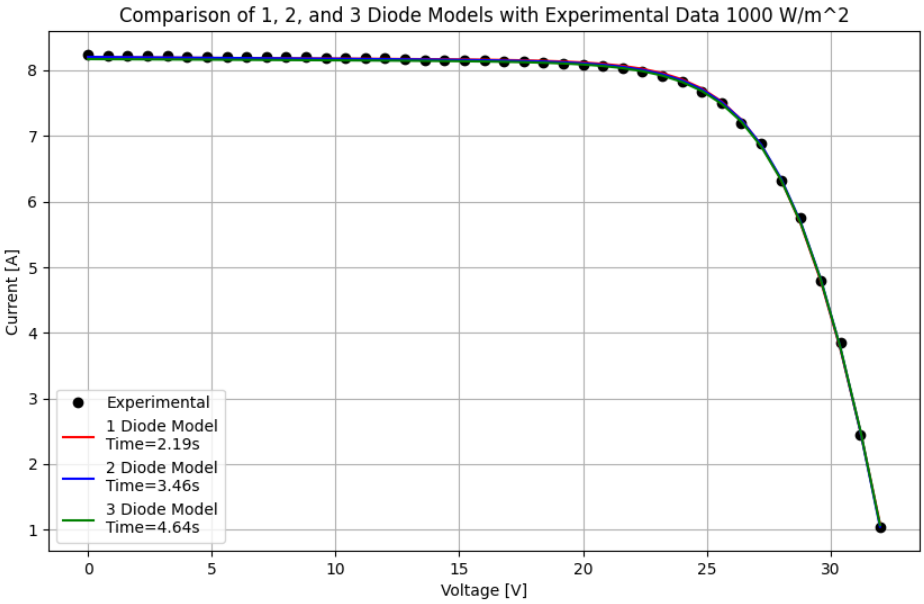

Figure 4. Comparison between the simulated I-V curves for the different diode models and the experimental data of the KC200GT module at 1000 W/m^2

portion of the curve. These differences are more pronounced in the more complex models, suggesting overfitting or sensitivity to parameter initialization in this region. Nevertheless, all models provide an adequate representation of the I-V behavior, validating the effectiveness of the proposed estimation methodology.

Table 9 presents the estimated values of the main electrical parameters *i.e.*, the series resistance (R_s), shunt resistance (R_{sh}), and diode ideality factors (n_1, n_2, n_3), as obtained through the hybrid EOA-NRM optimization for the single-, double-, and triple-diode models under irradiance levels of 1000, 800, and 400 W/m^2. This table does not compare the models against other optimization methods; it focuses on how the internal parameters vary depending on the model structure and irradiance conditions.

To evaluate the variability and sensitivity of these parameters, Table 10 reports the standard deviation of each parameter across the modeling approaches and irradiance levels. The results indicate that the shunt resistance (R_{sh}) exhibits the highest variability, suggesting that it is particularly sensitive to model structure and may play a compensatory role in fitting the experimental I-V data. Conversely, when present, the ideality factors n_2 and n_3 show lower variation under reduced irradiance, reflecting increased stability in the deeper layers of the multi-diode models.

Table 9. Parameters for each diode model, estimated via EOA-NRM at 1000, 800, and 400 W/m^2

Parameter	**1000 W/m^2**			**800 W/m^2**			**400 W/m^2**		
	SDM	**DDM**	**TDM**	**SDM**	**DDM**	**TDM**	**SDM**	**DDM**	**TDM**
R_s (Ω)	0.29139	0.27152	0.29792	0.22434	0.21767	0.34925	0.29851	0.34617	0.30368
R_{sh} (Ω)	515.92	393.04	483.51	554.47	462.57	472.94	566.92	490.82	492.95
n_1	1.4377	1.75619	1.61631	1.49353	1.45960	1.47853	1.42719	1.58566	1.71085
n_2	–	1.38294	1.58845	–	1.78404	1.77105	–	1.52005	1.51685
n_3	–	–	1.48960	–	–	1.60736	–	–	1.56716

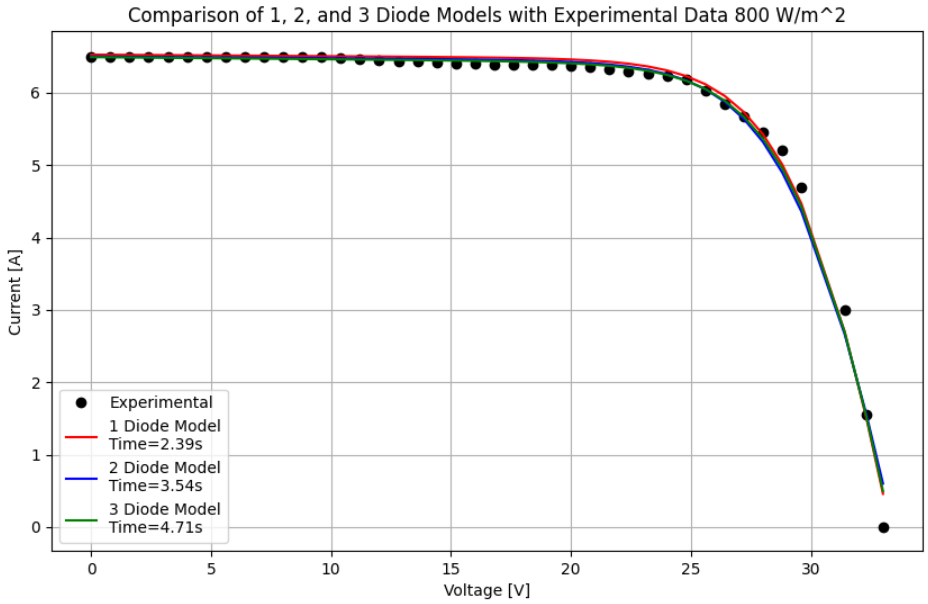

Figure 5. Comparison between the simulated I-V curves from the different diode models and the experimental data of the KC200GT module at 800 W/m^2

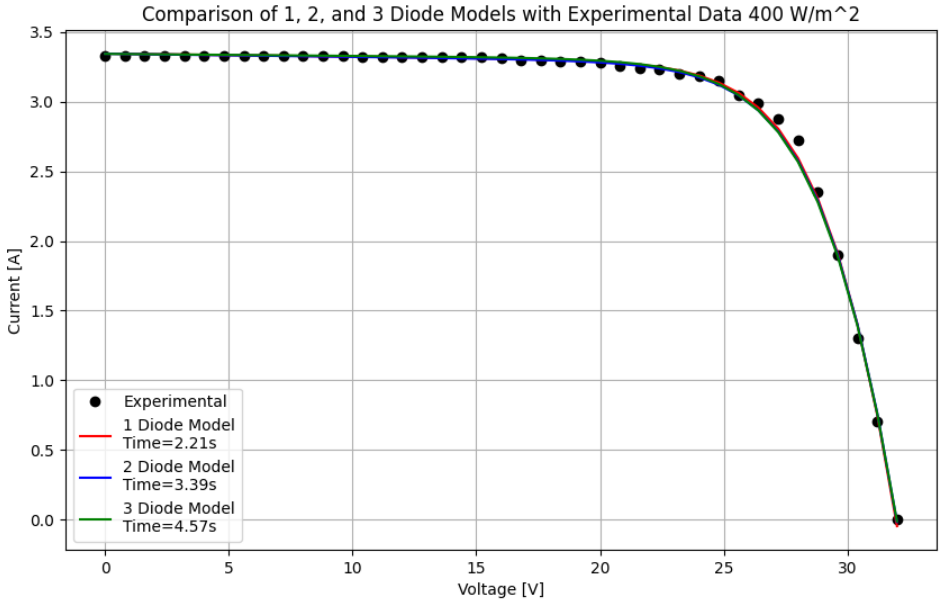

Figure 6. Comparison between the simulated I-V curves from the different diode models and the experimental data of the KC200GT module at 400 W/m^2

Table 10. Standard deviation of the parameters R_s, R_{sh}, n_1, n_2, and n_3 for each irradiance level

Parameter	**1000 W/m^2**	**800 W/m^2**	**400 W/m^2**
R_s (Ω)	0.0135	0.0582	0.0216
R_{sh} (Ω)	63.28	47.88	41.07
n_1	0.1596	0.0174	0.1475
n_2	0.1452	0.0068	0.0019
n_3	—	—	0.0209

As shown in Table 10, the shunt resistance (R_{sh}) exhibits the highest variability across all irradiance levels. This suggests that R_{sh} often plays a compensatory role during optimization, allowing different values of this parameter to yield similar RMSE outcomes. In the case of the TDM, this effect is amplified by the larger number of parameters, which increases the likelihood of coupling between them. Consequently, the objective-function landscape becomes relatively flat with respect to R_{sh}, explaining the instability and higher error observed for this model.

8. Conclusions and future work

This study proposed a hybrid parameter estimation methodology for PV cell modeling which integrates the global exploration capabilities of the EOA and the local refinement accuracy of the NRM. Implemented entirely in Python, this strategy was applied to the SDM, DDM, and TDM and validated using experimental data for the Kyocera KC200GT module.

A comparison of the results indicated that the double-diode configuration offers the most favorable trade-off between model simplicity and accuracy, achieving the lowest RMSE while faithfully reproducing the I–V behavior. The SDM provided a reasonable approximation near the open-circuit voltage, capturing the overall voltage range with fewer parameters. However, its simplified structure limited the accuracy across the entire I–V curve, making it less reliable than the DDM in terms of overall performance. In contrast, the TDM, despite its enhanced physical expressiveness, did not yield significant improvements and showed susceptibility to overfitting due to parameter coupling and the need for more iterations to converge. On the other hand, the algorithm itself demonstrated high accuracy but exhibited large variations in shunt resistance across all irradiance levels.

The use of the NRM as a numerical solver ensured a reliable convergence, particularly in the nonlinear regions near the maximum power point. Nonetheless, slight deviations were observed in this region for all models, possibly linked to high estimated shunt resistance values.

As future work, it would be valuable to investigate which model parameters could be more effectively controlled or constrained during the optimization process in order to ensure more consistent estimations, particularly regarding the resistive parameters. Since a high shunt resistance is essential for minimizing leakage currents and maintaining ideal cell performance, refining the algorithm to better guide this parameter within physically meaningful limits could enhance model reliability.

Acknowledgments

The authors acknowledge the support provided by Thematic Network 723RT0150, titled *Red para la integración a gran escala de energías renovables en sistemas eléctricos* (RIBIERSE-CYTED), funded by the 2022 call for thematic networks of the CYTED (Ibero-American Program of Science and Technology for Development). This research was also supported by Project No. 6-24-9, titled *Desarrollo de una metodología de control secundario para microrredes de corriente continua aisladas empleando control predictivo basado en el modelo*, managed by Universidad Tecnológica de Pereira's Vicerrectoría de Investigación, Innovación y Extensión.

REFERENCES

1. M. A. Navarro, D. Oliva, A. Ramos-Michel, and E. H. Haro, "An analysis on the performance of metaheuristic algorithms for the estimation of parameters in solar cell models," *Energy Conversion and Management*, vol. 276, p. 116523, Jan. 2023.
2. L. M. P. Deotti and I. C. da Silva Junior, "A self-started predictor–corrector method for calculating the lambert w function within the scope of the photovoltaic single diode model," *Solar Energy*, vol. 276, p. 112681, Jul. 2024.
3. A. Sabadus and M. Paulescu, "On the nature of the one-diode solar cell model parameters," *Energies*, vol. 14, no. 13, p. 3974, Jul. 2021.
4. K. Chennoufi, M. Ferfra, and M. Mokhlis, "An accurate modelling of photovoltaic modules based on two-diode model," *Renewable Energy*, vol. 167, pp. 294–305, Apr. 2021.
5. M. H. Qais, H. M. Hasanien, S. Alghuwainem, K. Loo, M. Elgendy, and R. A. Turky, "Accurate three-diode model estimation of photovoltaic modules using a novel circle search algorithm," *Ain Shams Engineering Journal*, vol. 13, no. 3, p. 101824, May 2022.
6. S.-S. Chen, Y.-T. Jiang, W.-B. Chen, and X.-Y. Li, "Terime: An improved rime algorithm with enhanced exploration and exploitation for robust parameter extraction of photovoltaic models," *Journal of Bionic Engineering*, vol. 22, no. 3, pp. 1535–1556, Apr. 2025.
7. N. J. L. Ballesteros, "Estimación de parámetros en máquinas y dispositivos eléctricos," Universidad Distrital Francisco Jose de Caldas, Tech. Rep., 1 2024.
8. I. Choulli, M. Elyaqouti, E. h. Arjdal, D. Ben hmamou, D. Saadaoui, S. Lidaighbi, A. Elhammoudy, and I. Abazine, "Hybrid optimization based on the analytical approach and the particle swarm optimization algorithm (ana-pso) for the extraction of single and double diode models parameters," *Energy*, vol. 283, p. 129043, Nov. 2023.
9. D. Yadav, N. Singh, V. S. Bhadoria, V. Vita, G. Fotis, E. G. Tsampasis, and T. I. Maris, "Analysis of the factors influencing the performance of single- and multi-diode pv solar modules," *IEEE Access*, vol. 11, pp. 95 507–95 525, 2023.
10. K. Ramakrishnan, B. Ajitha, and Y. Ashok Kumar Reddy, "Review on metal sulfide-based nanostructures for photodetectors: From ultraviolet to infrared regions," *Sensors and Actuators A: Physical*, vol. 349, p. 114051, Jan. 2023.
11. J. Park, C. Yu, S. Min, J. Shim, and D. Shin, "Extracting the inherent ideality factor of a diode from electrical current–voltage characteristics," *Electronics Letters*, vol. 59, no. 23, Nov. 2023.
12. M. J. Heredia-Rios, L. Hernandez-Martinez, M. Linares-Aranda, M. Moreno-Moreno, and J. F. Méndez, "Analysis of losses associated with series resistance (rs) in simple-structured c-si solar cells," *Energies*, vol. 17, no. 7, p. 1520, Mar. 2024.
13. S. Bader, X. Ma, and B. Oelmann, "One-diode photovoltaic model parameters at indoor illumination levels – a comparison," *Solar Energy*, vol. 180, pp. 707–716, Mar. 2019.
14. M. Calasan, S. Vujosevic, M. Alruwaili, and M. A. Ibrahim, "Optimization of four-diode equivalent circuit models for solar cells: Analytical formulation and performance enhancement," *Alexandria Engineering Journal*, vol. 127, pp. 411–430, Aug. 2025.
15. C. Chermite and M. Rachid Douiri, "Hybrid Tiki Taka and Mean Differential Evolution based Weibull distribution: A comprehensive approach for solar PV modules parameter extraction with Newton-Raphson optimization," *Energy Conversion and Management*, vol. 314, p. 118705, Aug. 2024.
16. K. Tifidat, N. Maouhoub, F. E. Ait Salah, S. Askar, and M. Abouhawwash, "An adaptable method for efficient modeling of photovoltaic generators' performance based on the double-diode model," *Heliyon*, vol. 10, no. 13, p. e33946, Jul. 2024.
17. K. Hong Min, H.-e. Song, M. Gu Kang, S. Hee Lee, and S. Park, "Double-diode model carrier lifetime-based internal recombination parameter analysis and efficiency prediction of crystalline si solar cells," *Solar Energy*, vol. 277, p. 112697, Jul. 2024.
18. E. Moshksar, "Two datasheet-based approaches for double-diode pv modeling with an efficient trade-off between accuracy and simplicity," *Heliyon*, vol. 10, no. 16, p. e36424, Aug. 2024.
19. A. M. Deaconu, D. T. Cotfas, and P. A. Cotfas, "Extracting photovoltaic cells parameters for three diode model using hsda algorithm," *Energy Reports*, vol. 12, pp. 5096–5109, Dec. 2024.
20. I. Cetinbas, "Parameter extraction of single, double, and triple-diode photovoltaic models using the weighted leader search algorithm," *Global Challenges*, vol. 8, no. 5, Apr. 2024.
21. M. A. Soliman, A. Al-Durra, and H. M. Hasanien, "Electrical parameters identification of three-diode photovoltaic model based on equilibrium optimizer algorithm," *IEEE Access*, vol. 9, pp. 41 891–41 901, 2021.
22. O. D. Montoya, W. J. Gil-González, and J. M. López-Lezama, "Vortex search algorithm applied to the parametric estimation in pv cells considering manufacturer datasheet information," *IEEE Latin America Transactions*, vol. 19, no. 9, pp. 1581–1589, Sep. 2021.
23. L. Wang, Q. Yuan, B. Zhao, B. Zhu, and X. Zeng, "Parameter identification of photovoltaic cells/modules by using an improved artificial ecosystem optimization algorithm and newton-raphson method," *Alexandria Engineering Journal*, vol. 123, pp. 559–591, Jun. 2025.